Fusion Engineering and Design 218 (2025) 115190

Contents lists available at ScienceDirect

Fusion Engineering and Design

journal homepage: www.elsevier.com/locate/fusengdes

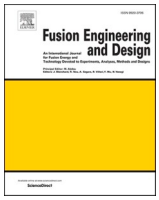

Test of RANS turbulence models for application on ribbed duct flows by comparison to experimental flow field and heat transfer data

S. Gordeev *, F. Arbeiter, S. Ruck

Karlsruher Institut für Technologie, Campus Nord, Eggenstein-Leopoldshafen, Germany

ARTICLE INFO

Keywords:
Fusion
First wall
Helium
Heat transfer
CFD
Turbulence models

ABSTRACT

The aim of the study is to find the most accurate and robust CFD solution that can be applied to cases with flow separation and heat transfer induced by ribs.

The first part of the paper analyses the ability of six Reynolds-Averaged Navier Stokes (RANS) models to reproduce the separated air flow (isothermal) in a transversally ribbed rectangular channel, in comparison to flow field data measured with Laser Doppler Anemometry.

In the next step the models were evaluated in the prediction of convective heat transfer and pressure drop in v-ribbed heated gas cooling channel measured in HETREX-PT (HEat TRansfer Enhancement eXperiments - Pressure, Temperature) experiments at KIT, with a channel geometry close to the intended application.

Turbulence models such as standard k-ω SST (SST) and Realisable k-ε model (KE-RE) as well as models derived on the basis of the elliptic blending approach: Reynolds Stress model (RSM), $v2$-f model (V2F), Elliptic Blending model (KE-EB) and Lag-Elliptic Blending model (KE-LAG-EB) were selected.

The flow conditions (flow rate, heating power) were scaled from helium flow in HCPB (P=8MPa Tin=300 °C) to air at 0.4 MPa and 24 °C by the two similarity quantities Reynolds number and the dimensionless heating rate q^{+}. The rib-arrays consist of upstream pointing transversally oriented 60° V-shaped ribs. The comparative analysis of the turbulence models deals with the investigation of the distribution of vortex structures caused by ribs and their influence on heat transfer.

The flow between attached ribs calculated by k-ω SST is almost completely detached, leading to a significant under-prediction of heat transfer. The standard k-ε model underestimates the turbulence production at the leading edge and in the shear layer over the recirculation region and, thus, the heat transfer between the ribs. The elliptical blending models give results that are closer to the measurements. The RSM, V2F and KE-EB models perform better agreements with experimental data. The V2F model provides the best prediction and is found to be most suitable for the simulation of heat transfer in the presented rib-structured channel flow.

1. Introduction

One of breeding blanket concepts for the European DEMOnstration reactor (DEMO) is Helium Cooled Pebble Beds (HCPB) uses helium to cool down the First Wall (FW) [1,2]. The main function of the FW is to contribute to electrical production by removing high heat flux from the plasma with an effective coolant system. The thermal power assumes a homogeneous FW heat flux of typically 0.3 MW/m^2, with the possibility of excursions to much higher values. The structural material of the blanket is the ferritic-martensitic 9 % Cr 1 % W steel grade Eurofer97. The pressurized helium gas (at 8 MPa) has inlet/outlet temperatures of 300/520 °C. Helium gas has the advantages of chemical and radiological inertness in the FW application. Typical for gases low density and thermal conductivity requires thermo-hydraulically enhanced surface designs for the cooling channels to improve heat transfer and ensure operation within temperature limits. The macro-roughness of the duct walls of gas-cooled FW applications to improve heat transfer has been investigated for different surface structure designs [3,4]. The turbulent flow and heat transfer of cooling channels roughened by upstream pointing V-shaped fins have been analysed numerically and experimentally [5–8]. The geometric family of upstream-pointing v-shape ribs with filleted edges (termed “AV2” in the present project) is a candidate for application in the FW channels due to their experimentally proven high thermal-hydraulic performance and their compatibility with the

* Corresponding author.
E-mail address: sergej.gordeev@kit.edu (S. Gordeev).

https://doi.org/10.1016/j.fusengdes.2025.115190
Received 30 January 2025; Received in revised form 28 March 2025; Accepted 13 May 2025
Available online 24 May 2025

manufacturing strategy of the FW.

The flow on component-level is affected by hydraulic and thermal development and lack of exploitable symmetry Therefore, to enable reliable thermal hydraulic analyses of FW cooling channels (1-2 m channel length), it is crucial to quantify the applicability of existing CFD models such as Reynolds-Averaged Navier Stokes (RANS) models to capture the relevant flow specifics occurring in duct flows and assure the quality and reliability of predictions. The aim of this study is to test the different turbulence models that may be used in the thermal analysis of FW cooling. The second important part of the report is the analysis of flow structures in V-shaped channels, which have a significant influence on heat transfer (HETREX-PT experiments [9,10]).

The applicability of six RANS models using the commercial CFD software (Star-CCM+ [11]) was examined for the prediction of the heat transfer and pressure drop in the ribbed gas cooling channel measured in theHETREX-PT (HEat TRansfer Enhancement eXperiments - Pressure, Temperature) experiments.

2. Tested turbulence models

The six models used come from different subcategories of the RANS models and were selected to test the widest possible range of RANS models.

Namely the following turbulence models have been used:

k-ω SST (SST) turbulence model
Elliptic Blending Reynolds Stress model (RSM)
v2-f model (V2F)
k-ε Realisable model (KE-RE)
k-ε Elliptic Blending model (KE- EB)
κ-ε Lag-Elliptic Blending model (KE-LAG-EB)

The *k-ω* SST (SST) turbulence model [12]:

The *k-ω* SST (SST) turbulence model combines two models, the *k-ω* and the *k-ε* using a blending function (which includes functions of wall distance) that would include the diffusion term far from walls, but not near the wall.

The *k-ε* Realisable model (KE-RE) [13]:

In contrast to the standard k-ε model the KE-RE model contains a new transport equation for the turbulent dissipation rate ε. The KE-RE model implementation in Star-CCM+ combines the Realizable k-ε model with the two-layer approach.

The *v2-f* Model (V2F) [14]:

The V2F turbulence model solves transport equations for two more turbulence quantities in addition to *k* and *ε*, namely the wall-normal stress component v^2 and the elliptic relaxation parameter *f*, in order to determine the turbulent eddy viscosity. The model has been already successfully used for simulating separated flows, three dimensional configurations and flows with heat transfer [15–20].

The *k-ε* Elliptic Blending model (KE-EB) [21]:

The aim of the KE-EB turbulence model is to stand as a code-friendly version of the V2F model. This eddy viscosity model solves for k and ε as turbulence variables, representing respectively the turbulent kinetic energy and its dissipation rate, as well as two non-dimensional variables, $\varphi=(v^2)/k$ and α. The first of these latter two represents the ratio of wall normal Reynolds stress to turbulent kinetic energy (thus being a measure of the near-wall turbulence anisotropy) and the second is a wall proximity sensitive quantity (i.e. it takes the value 0 at a wall and 1 in the far field). The coefficient α is solved for via an elliptic equation (L representing the turbulence length-scale): α-L2 ∂jj α=1. It is used as a blending parameter in the ¯(ϑ2) source term modelling to feature a smooth transition between near-wall and quasi-homogeneous models.

The κ-ε Lag-Elliptic Blending model (KE-LAG-EB) [22]:

The Lag Elliptic Blending model is derived based on Reynolds-stress model, using the concept of the lag between stress and strain in combining with the standard Elliptic Blending (KE-EB) model.

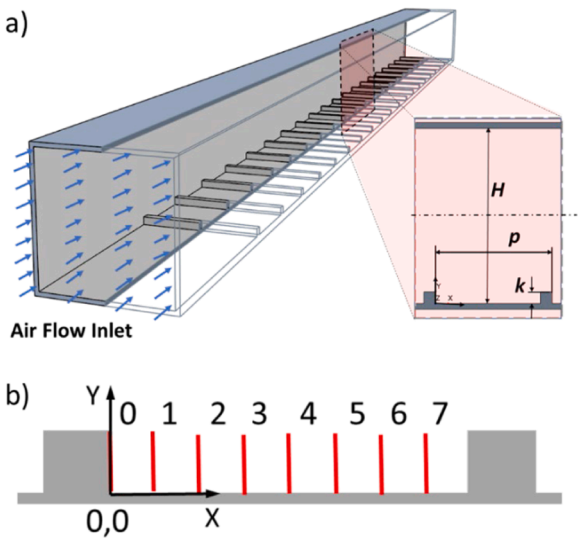

Fig. 1. a) Sketch of the test section and nomenclature of the rib configuration [28], b) x/*k* position of LDA-measurement cross sections.

In flow regions with non-equilibrium effects, linear eddy viscosity models tend to overpredict the production of turbulent kinetic energy. The KE-LAG-EB model is able to predict the misalignment of the principal components of the stress and strain-rate tensors. The KE-LAG-EB model provides a good predictive capability for separated or unsteady flow

The Elliptic Blending Reynolds Stress model (RSM) [23]:

RSM models have the potential to predict complex flows more accurately than eddy viscosity models because the transport equations for the Reynolds stresses naturally account for the effects of turbulence anisotropy and streamline curvature [24–27]. The Elliptic Blending RSM model, like the other second-moment closure models, directly calculates the components of the Reynolds stress tensor by solving the governing transport equations. The RSM model is based on an inhomogeneous near-wall formulation of the quasi-linear quadratic pressure-strain term. The blending function is used to blend the viscous sub-layer with the log-layer formulation of the pressure-strain term. This approach requires the solution of an elliptic equation for the blending parameter α. The pressure-strain model is based on a blending of near-wall and quadratic pressure strain models for the pressure-strain and dissipation.

3. Validation of turbulence models for isothermal transversal rib flows

3.1. Experimental setup

Validation of turbulence models on similar experiments can provide an idea about the ability of the selected models to estimate flow behaviour and turbulence structures.

Laser Doppler anemometry (LDA) measurements in the fully developed turbulent flow at Reynolds number of 5×10^4 through a one-sided transversally ribbed square channel [28] were compared with simulations.

The test section consisting from the 60×60 mm^2 square channel is schematically depicted in Fig. 1a. The length of the test section was 1180 mm. The bottom wall of the channel was periodically structured by ribs with a 4×4 mm^2 square cross section and a distance between the ribs of 36 mm. Measurements were taken at different positions in the region $0 \leq x/k \leq 8$, where k is the rib height (see fig. 1b).

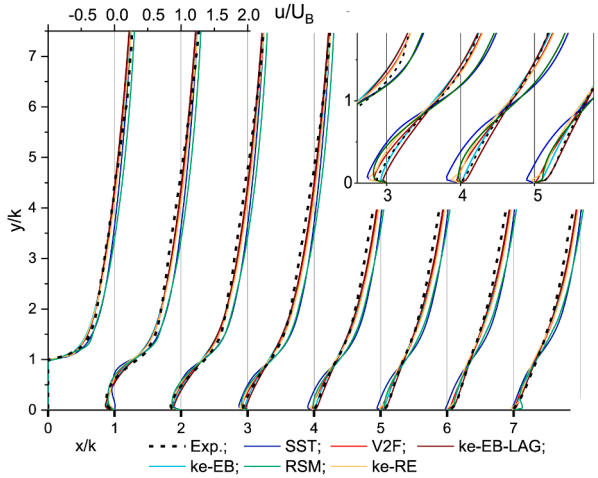

Fig. 2. . Normalized streamwise velocity u/U_b distribution at different streamwise positions compared with measurements [28].

3.2. Mesh and boundary conditions

A part of the channel section including three ribs was modelled with 13.5 million hexahedral cells. The near wall area was resolved with 20 cell layers. The value of the dimensionless wall distance $y^+ = yu_\tau/\nu$ in the first cell layer on the wall does not exceed 0.2. Here u_τ is the friction velocity defined as $u_\tau = \sqrt{(\tau_w/\rho)}$, where ν is the kinematic viscosity. Therefore, all turbulence models used are suitable for the low-Re treatment of the near-wall area.

The liquid was treated as an incompressible air stream at pressure and temperature measured at the inlet to the test section.

Inlet and outlet were modelled as interface with periodic boundary conditions and streamwise bulk velocity U_b=12.67 m/s. At wall boundaries smooth and a no-slip boundary condition were selected.

All wall surfaces of the channel flanges have adiabatic boundary conditions.

3.3. Simulation results

The solution was considered to be converged when all normalized residuals were lower than 1×10^{-4}, and monitors of velocity components and turbulence parameters were constant.

The streamwise velocity u, turbulent kinetic energy TKE and Reynolds shear stresses $\overline{u'v'}$ normalized by bulk velocity U_b and its squared value U_b^2, respectively, were compared with measurements.

For RANS models, Reynolds stresses are computed from the eddy viscosity, μ_t, determined from the Boussinesq approximation. RSM approximates Reynolds stresses from flow properties and, hence, the six Reynolds stresses can be extracted from simulation results. For comparison with LDA measurements, the components of turbulence intensity and the Reynolds shear stress are estimated from the following equations:

$$U' = \sqrt{\overline{u'u'}} = \sqrt{\frac{\mu_t\left[\frac{\partial u}{\partial x}+\frac{\partial u}{\partial x}\right]-\frac{2}{3}\left[\rho k+\mu_t\frac{\partial u}{\partial x}\right]}{-\rho}} \quad (1)$$

$$V' = \sqrt{\overline{v'v'}} = \sqrt{\frac{\mu_t\left[\frac{\partial v}{\partial x}+\frac{\partial v}{\partial x}\right]-\frac{2}{3}\left[\rho k+\mu_t\frac{\partial v}{\partial x}\right]}{-\rho}} \quad (2)$$

$$U'V' = \overline{u'v'} = \frac{\mu_t\left[\frac{\partial u}{\partial y}+\frac{\partial v}{\partial x}\right]}{-\rho} \quad (3)$$

Velocity gradients $\partial u/\partial x$, $\partial v/\partial x$, $\partial u/\partial y$, $\partial v/\partial x$, and eddy viscosity, μ_t are direct Star-CCM+ outputs while ρ is the density of air. The turbulent kinetic energy is composed of the Reynolds normal stresses $TKE = 1/2(\overline{u'^2} + \overline{v'^2} + \overline{w'^2})$. Because the measurements could only be performed in streamwise (x) and wall-normal (y) directions; for comparison with experimental data, TKE was obtained without the Reynolds stress component $\overline{w'^2}$.

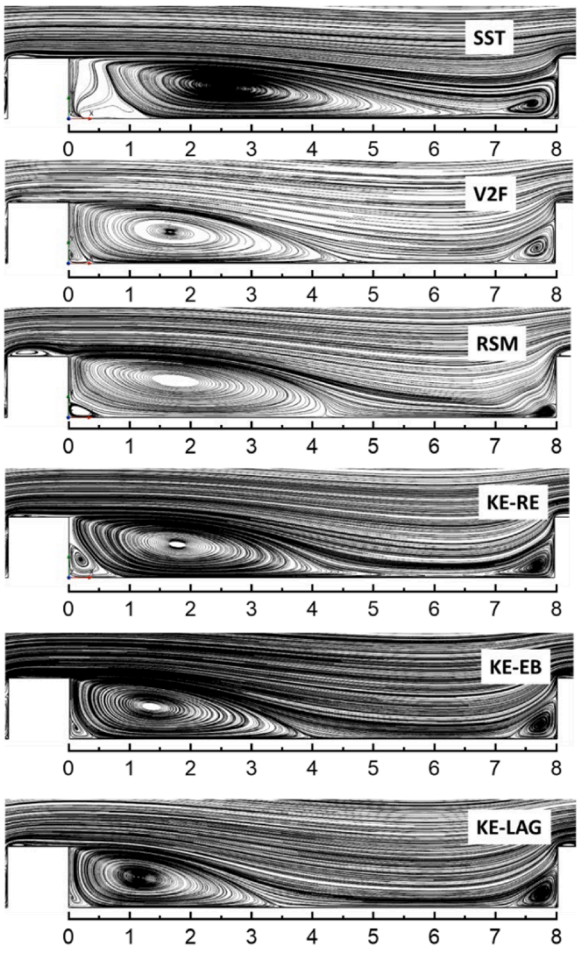

Fig. 3. . Flow separation region between two ribs visualised by velocity stream lines.

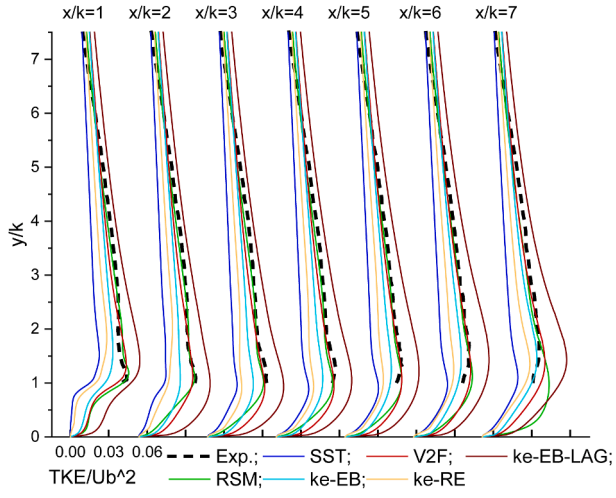

Fig. 4. Distribution of normalized turbulent kinetic energy TKE/U_b^2 at different streamwise positions compared with measurements [28].

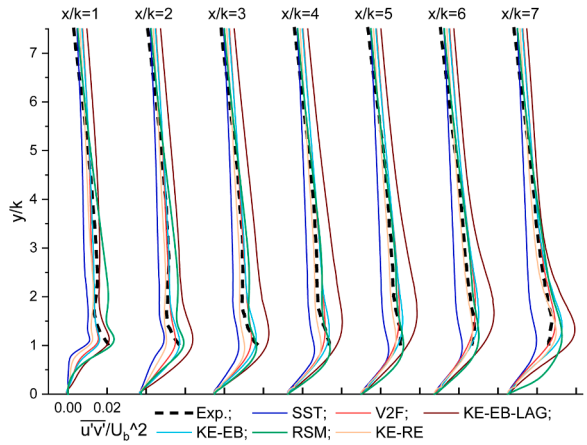

Fig. 5. . Distribution of normalized Reynolds shear stresses $u'v'/U_b^2$ at different streamwise positions compared with measurements [28].

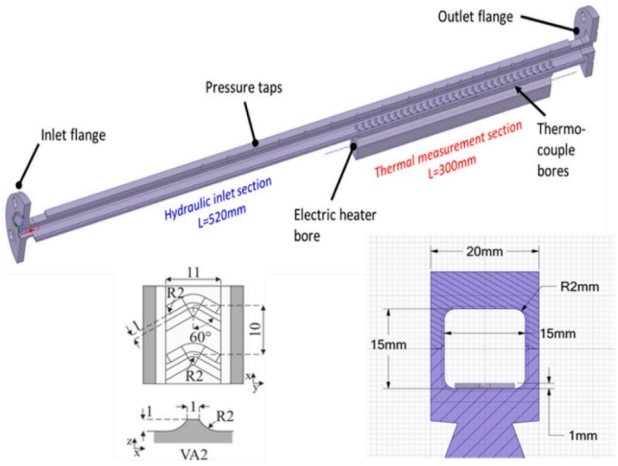

Fig. 6. CAD model of HETREX test section.

Comparison of simulations and experimental data are shown in Figs. 3-6. Geometric dimensions are normalized over the rib height *k*.

Figs. 2 and 3 presents the velocity development of the flow between ribs obtained in the middle of the channel (z=0). As it can be seen from Figs. 2 and 3 the flow pattern prediction is fairly well returned by V2F, RSM, KE-EB and KE RE models. In contrast to the KE-EB-LAG model, which slightly underestimates the length of the large recirculation bubble, the SST model provides an excessively long recirculation area and noticeably fails to predict the recovery length.

Minor differences between the RSM and *k-ε* based models can be observed in the velocity profiles. For all of these models the recirculation length, where the streamwise velocity near the wall($y/k < 0.5$) is switched from negative to positive value is predicted by x/k=4, while by the SST the negative velocity can be observed at x/k=6. The best prediction is shown by the KE-EB-LAG and KE-EB models followed by RSM and V2F.

Figs. 4 and 5 show the profiles of the turbulent kinetic energy (*TKE*) and turbulence shear stress. The comparison of *TKE* and Reynolds shear stresses profiles confirm the quality of the V2F predictions. The peak of the turbulent intensity is well predicted by the V2F model on the whole length between ribs. However, in the recirculation region the model slightly underestimates the y/k position of maximum kinetic energy. This mostly concerns the RSM model, the maximum of which noticeably shifts downwards, approaching the next rib. The KE-EB and KE-EB-LAG models also show relatively good agreement with the measurements, although both do not clearly show the TKE maximum at the beginning of

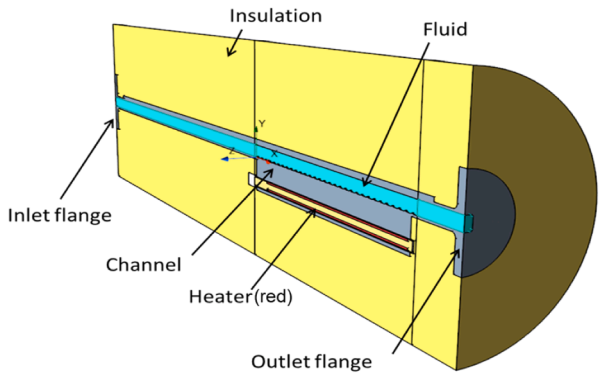

Fig. 7. Computational domain of the test section.

the flow separation ($0<x/k<2$). While the KE-EB model underestimates the turbulent intensity in the shear layer at x/k=1, the KE-EB-LAG overestimates it over almost the entire length. The results using the KE-RE and SST models do not capture the development of turbulent kinetic energy and Reynolds shear stress at all. When the KE-RE model approaches the measured results at $x/k>5$, the SST model significantly underestimates the degree of turbulent intensity along the entire length between the ribs.

The turbulence models with elliptic blending function consistently show predictions of the TKE close to the experiment with the exemption of ke-EB-LAG which showed an overprediction by about 30 %.

It is interesting to compare two relatively similar models, KE-EB and KE-EB-LAG regarding the terms and constants of the *k-ε* system on which they are based.

In contrast to the KE-EB, the KE-EB-LAG model is based on the elliptic blending-Reynolds stress model (EB-RSM) and takes into account the delay between the stress and the strain tensor. For this reason the KE-EB-LAG model provides a good predictive capability for separated or unsteady flow [22]. Another important difference between the KE-EB and KE-EB-LAG models implemented in StarCCM+ is the definition of the coefficient of the destruction term $C_{\varepsilon 2}/C_{\varepsilon 2}^*$ in the dissipation equation. In KE-EB model, this term is defined as a function of the turbulent kinetic energy gradient, to reduce the value of $C_{\varepsilon 2}$=1.83 in the shear layer, where the free-stream is starting to dominate. In contrast to the original KE-EB-LAG turbulence model described in [22], in StarCCM+ the constant value of $C_{\varepsilon 2}$=1.9, yields too high turbulence growth rate therefore an under predicted recirculation size.

4. Validation of turbulence models for heated v-rib flows

4.1. Description of the test section HETREX-PT

The HETREX-PT experiments are documented in [9,10]. HETREX-PT aimed at providing experimental data with the primary objective to directly compare a number of FW channel geometry options in terms of heat transfer and pressure drop. The test section (See Fig. 7) represented a channels fabricated of stainless steel, equipped with an array of thermocouples and heated with a commercial off-the-shelf cylindrical heater cartridge. The flow conditions (flow rate, heating power) were scaled from helium 8MPa 300 °C to air at 0.4 MPa and by the similarity

Table 1
Inlet conditions.

Pressure at the exit flange x_h=370mm, p	[Pa]	395321.1
Inlet temperature, T_{IN}	[K]	297.09
Mass flow rate for half cross section, $\dot{m}$	[Kg/s]	0.01369
Estimate for half heater power, P_{eff}	[W]	114.76
Dimensionless parameters:		
Inlet Reynolds number	Re	104871.0
Dimensionless heating rate *	q^+	0.00103

quantities such as the Reynolds number and the dimensionless heating rate q+ (see below). The data were obtained from pressure ports and thermocouples in the global coordinate system of HETREX-PT. This analysis focused on the measurements in the channel with V-shaped ribs on the heated wall. Temperature and pressure drop measurements have been compared with CFD simulation results. The experimental method, detailed results and uncertainty discussion was described in [29], where also plots of the data for 21 different Reynolds numbers between 50000 and 250000 are shown with error bars. For the present case described in Table 1 at Re=104871 the expanded uncertainty range (k=2) for θ(x=180mm) is 8.3 % for the uncertainty contributions of heating power and temperatures. Uncertainty in the effective length of the heater is an additional possibly relevant contribution that could not yet be quantified.

4.2. Computational domain of HETREX-PT test section and boundary conditions

The geometry of the modelled test section is shown in Fig. 7. The model includes the full length structured channel with V-shaped ribs, external insulation and heater consisting of heated volume, MgO electrical insulator and steel jacket. Since the test section to be tested is symmetrical in the x-y plane, the steady state simulation gains in accuracy if the CFD model is only created as a half with symmetrical conditions of the test section but with a finer mesh.

4.3. Inlet and boundary conditions

In order to provide realistic flow conditions at the inlet, the flow parameters such as static pressure, velocity components and turbulence characteristics were obtained from the separate simulations of the air flow through the pipe contraction part that provides connection between the cylindrical pipe and the rectangular inlet channel of the test section. The structured mesh consists of 1.87e6 fluid cells. To ensure the required input parameters for all turbulence models, simulations of the inlet were carried out with two turbulence models: SST and RSM.

Inlet conditions are listed in Table 1.

$$*q^{+} = \frac{\dot{q}A_{Q}\beta}{\dot{m}C_{p}}, \beta = 1/T$$

All solid parts have contact interfaces with zero contact resistance with each other. The outer surfaces of the channel flanges have adiabatic boundary conditions. Convective boundary conditions with a heat transfer coefficient of 2.2 W/K/m^2 were applied to the outer surface of the insulation. The ambient temperature is set to 298K. The heating power was distributed homogeneously over the entire volume of the heater over the length of 270 mm.

4.4. Mesh

Two automatic volume mesh formats supported in Star-CCM+, Polyhedral and Trimmed meshes have been tested for the grid study. Near wall area and regions within the smooth parts of the channel are meshed by prismatic cells created by cell extrusion.

Both mesh types belong to the unstructured cell grids. It is known, CFD solvers converge better and can produce more accurate results when the grid is aligned with the predominant flow direction. Alignment in a structured grid is achieved almost implicitly because grid lines follow the contours of the geometry, whereas there's no such alignment in an unstructured mesh. On the other hand, unstructured meshes offer better flexibility for geometrically complex applications. Furthermore, they are much less sensitive to stretching since their typically irregular shape is not a restriction for several CFD codes. The final argument for the unstructured grid is, if the resulting vortices and secondary flows within a complex geometry affect the flow behaviour, the alignment of the cell to the streamlines will hardly be possible.

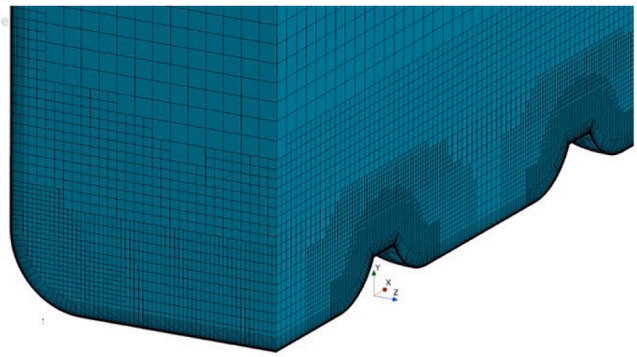

Fig. 8. Fine Trimmed Cell resolution of the flow domain, ribbed channel at the heating start.

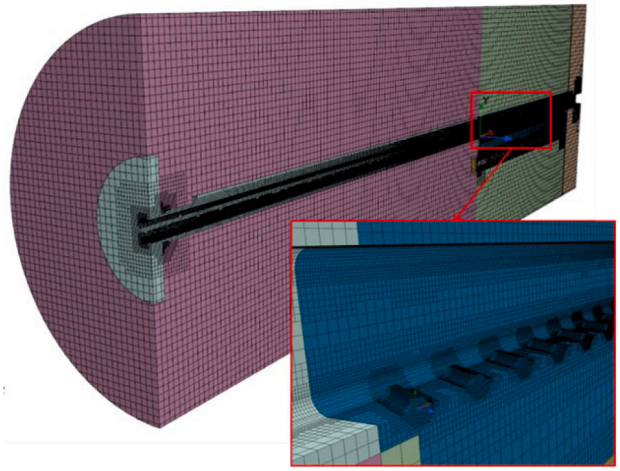

Fig. 9. Trimmed cell meshing of solid parts.

Comparative calculations were carried out on different coarse and fine fluid grids, which have a different core flow resolution and near-wall resolution. Solid meshes consisting of about 2.0e6 trimmed cells remained unchanged in all cases. Two turbulence models SST and RSM were used in the grid study. For the grid study all models adopt an "all-y^+ "wall treatment that employs blended wall functions to provide valid boundary conditions for flow, energy, and turbulence quantities across a wide range of near-wall mesh refinements. The number of fluid cells from "coarse" to "fine" varied between 2.8e6 and 35.0e6, the thickness of the wall-mesh region was between 1.0 and 0.375 mm respectively. The variation of the boundary layer resolution was 15 to 25 cell layers.

As mentioned, the solver can provide more accurate results if the grid is aligned at least to the main flow direction of the channel. Alignment in a trimmed grid is achieved because grid lines follow the main flow direction, while in polyhedral meshes there is no such alignment. Another problem is that polyhedral cells require a considerable number of neighborhood relationships compared to (trimmed) hexahedral cells, leading to resource-expensive solutions.

The grid independency study showed the need of further refining of the polyhedral mesh. Therefore it makes no sense to use a polyhedral grid because increasing grid resolution would increase computing time. Taking into account the requirement of y^+ maximum $\leq$1 for the low-Re wall treatment, the fine trimmed cell grid was selected for further simulations.

Fig. 8 shows the fragment of the flow region resolved with "Fine" trimmed cells used for further simulations. The solid area was also meshed using the same meshing method, as shown in Fig. 9.

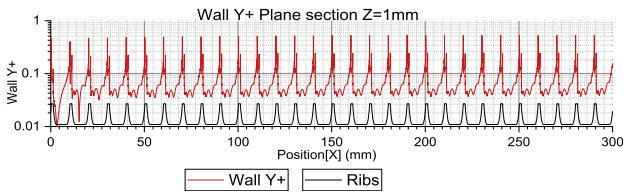

Fig. 10. Distribution of non-dimensional wall distance y^+, trimmed cells, fine grid resolution.

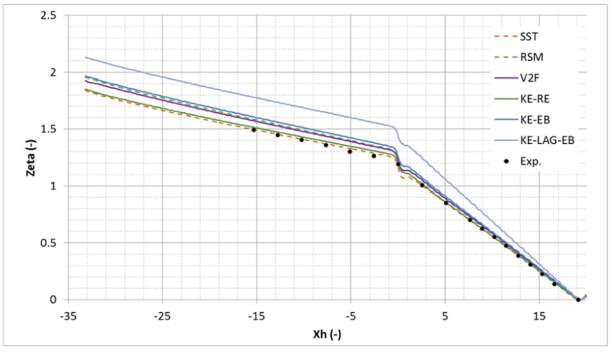

Fig. 11. Distribution of normalized pressure drop profiles (heated part from X_h=X/d_h=0).

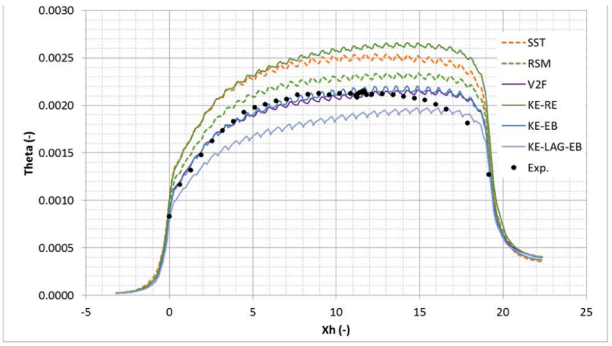

Fig. 12. Distribution of normalized temperature profiles.

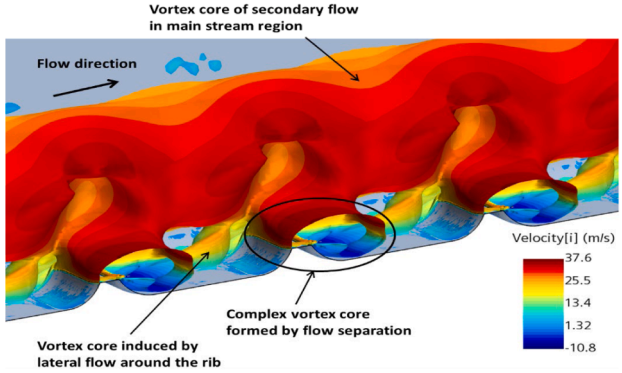

Fig. 13. Vortex core distribution of secondary flows (visualised by isosurface of λ2=-100).

Fig. 10 displays the distribution of y^+ values at the fine grid resolution to demonstrate the variation of y^+ along the ribbed wall.

4.5. Simulation results

The numerical solutions were regarded as converged when the normalized residuals became ≤10.e(-5).

The normalised pressure drop and temperature profile in the heated channel were used as a metric for the study, with the normalized pressure profile (Zeta):

$$\zeta(x) := \frac{p(x) - p(x = 300mm)}{\frac{1}{2\rho_{air}(p(x=300mm),T_{OUT})}\cdot\frac{\dot{m}^2}{A_Q^2}}$$

and the normalized temperature profile (Theta):

$$\theta(x) := \frac{T_A(x) - T_{IN}}{P_{eff}}\cdot\frac{A_{W,nom}}{d_h}\cdot\lambda_{air}(T_{IN})$$

where T_A is the mean temperature of the cross section, P_{eff} - effective heating power and$\rho_{air}$and λ_{air} – density and heat conductivity of air.

The axial coordinate used in the plots is normalised by the hydraulic diameter to allow comparison among reported results with different channel cross sections.

The nominal values of the geometry constants in the above equations are:

Hydraulic diameter, $d_h = 15.67{\cdot}10^{-3}m$

Flow cross section (without ribs), $A_Q = 221.6{\cdot}10^{-6}m^2$

Nominal heated area, $A_{W,nom} = 6{\cdot}10^{-3}m^2$

Diagrams in Fig. 11 and 12 present comparison of non-dimensional pressure and wall temperature calculated using six previously mentioned turbulence models.

All turbulence models overpredict the measured pressure drop. The best match is reached by the SST and KE-EB simulations, which overpredict ζ(X_h=0) by 2 %. Less accurate are KE-EB, V2F and RSM simulation results with the deviation from the measured pressure of 5 %. The KE-LAG-EB model shows the greatest overestimation of the pressure loss at 20 %.

The best match to the measured temperature is reached by the KE-EB, RSM and V2F models. While the RSM, KE-EB and V2F models overestimate the temperature with a maximum deviation of 12 % at the end of the heated length, the KE-LAG-EB model underestimates the temperature at the beginning of the heating with about the same deviation. In the central area of the heated length, the deviation is around 5 %. The RSM model overestimates the temperature at the end of the heated length by about 17 %. KE-RE and SST models provide the most inaccurate results with an overestimation of the temperature by more than 20-25 %.

Regardless of the quantitative results from different turbulence models, some of the features that are similar for all models should be highlighted:

- Pressure drop and wall temperature cannot be predicted accurately by any model. As to be expected, models that predicted high pressure drop (high momentum transfer) also predict low wall temperatures (high heat transfer).
- For all turbulence models, the temperature of the wall along the heated length differs in shape from the measured temperature profiles. Experimental measurements show that the maximum wall temperature is located near the middle of the heated length. The computed wall temperatures show their maximum nearer to the channel exit. This is a typical temperature profile for the constant heat flux along the heating length in the cooling channel.

The reason for these differences still needs to be investigated, including from an experimental perspective. Obviously, various

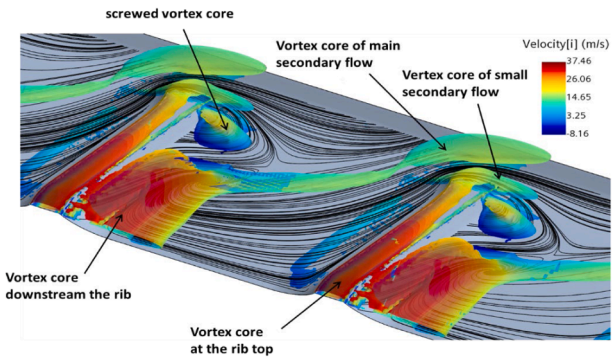

Fig. 14. Distribution of vortex cores close to the ribbed wall (V2F-simulation results). Isosurface of λ2=-1.5e7 with the color contour of main flow velocity. (For interpretation of the references to color in this figure legend, the reader is referred to the web version of this article.).

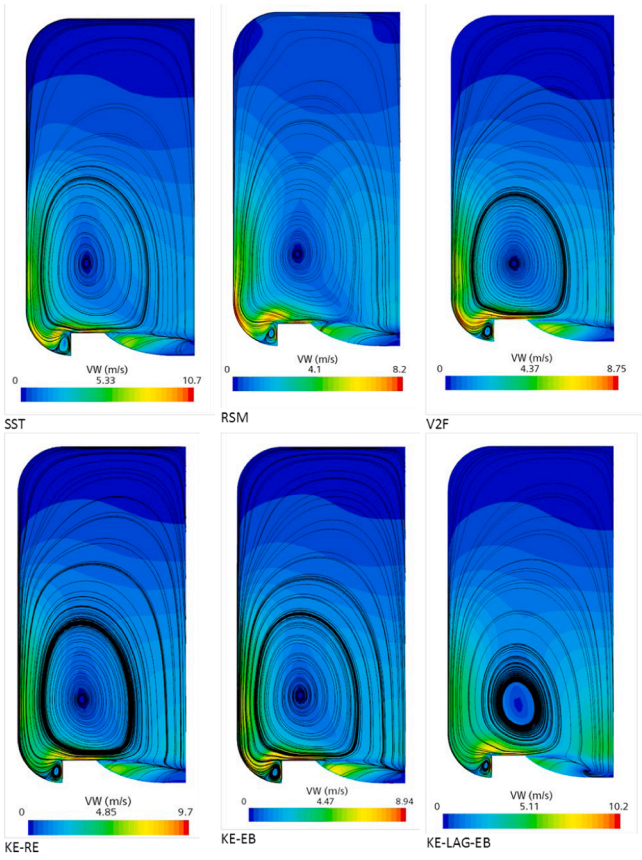

Fig. 15. Streamline plane section x=143 mm; Color scale magnitude of velocity components *V* and *W*. (For interpretation of the references to color in this figure legend, the reader is referred to the web version of this article.).

technical problems can affect the measurements.

From the simulation side, there are some considerations that explain these discrepancies and, despite the differences, enable further validation comparisons, since all tested turbulence models assume the same boundary conditions:

- The material properties and contact conditions could differ from the real values;
- The heating power distribution in the heater could deviate from the assumption about the constant heating power over the heating length;

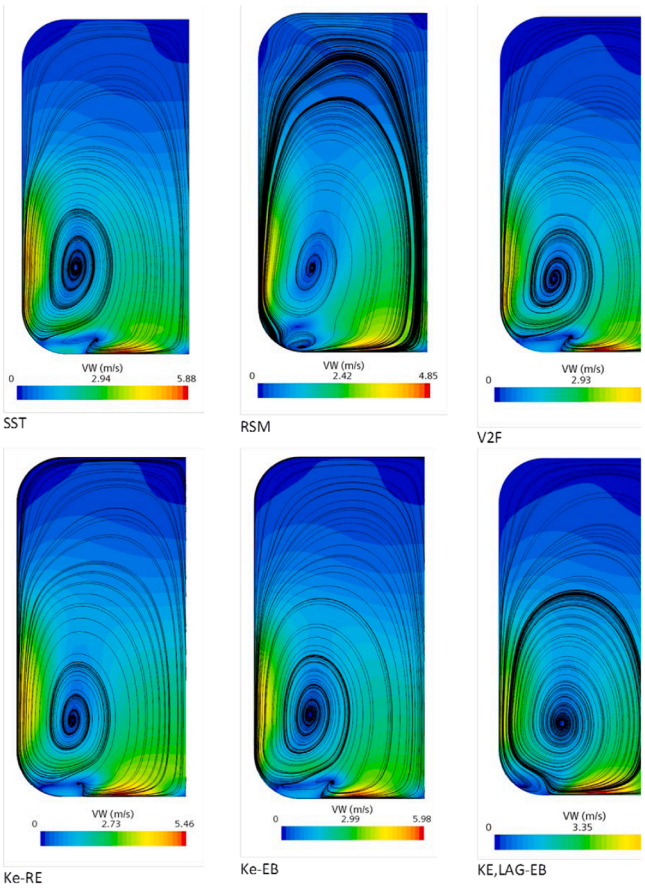

Fig. 16. Streamline plane section x=147 mm; Color scale magnitude of velocity components *V* and *W*. (For interpretation of the references to color in this figure legend, the reader is referred to the web version of this article.).

5. Analysis of flow structure and heat transfer in the channel flow

In the case of V-shaped ribs, the inclination of the ribs creates complex three-dimensional secondary flow structures. This significantly increases the heat transfer in the region of the ribs.

Figs. 13 and 14 show the vortex core distribution in the ribbed channel obtained from KE-RE simulations. The large scale eddy structure is visualisided by iso-surface counter of the second invariant of velocity gradient λ2 (Jeong and Hussain [30]). The vortex core surface is the iso-surface of the $\lambda 2$ criterion ($\lambda 2$=-100). The color of the vortex core surface is the contour of the velocity component of the fluid in the flow direction.

The vortex cores are located in the lower half of the channel above the ribbed wall. The regions are clearly visible (the symmetry condition must be taken into account):

(1) the large-scale vortex core of secondary flow in the main flow region, which represents the secondary flow in the channel;
(2) the vortex core area, which consists of two flow separation regions at the leading and trailing edges of the ribs;
(3) the vortex flow that develops along the ribs from the center of the channels and encloses the large secondary flow at the side wall.

Figs. 15 and 16 show the velocity field perpendicular to the flow direction $(V^2+W^2)^{0.5}$ combined with the representation of the streamlines in the cross sections above the top of the ribs (x=143 mm) and between the ribs (x=147 mm).

Resulting from simulations with the applied turbulence models, the

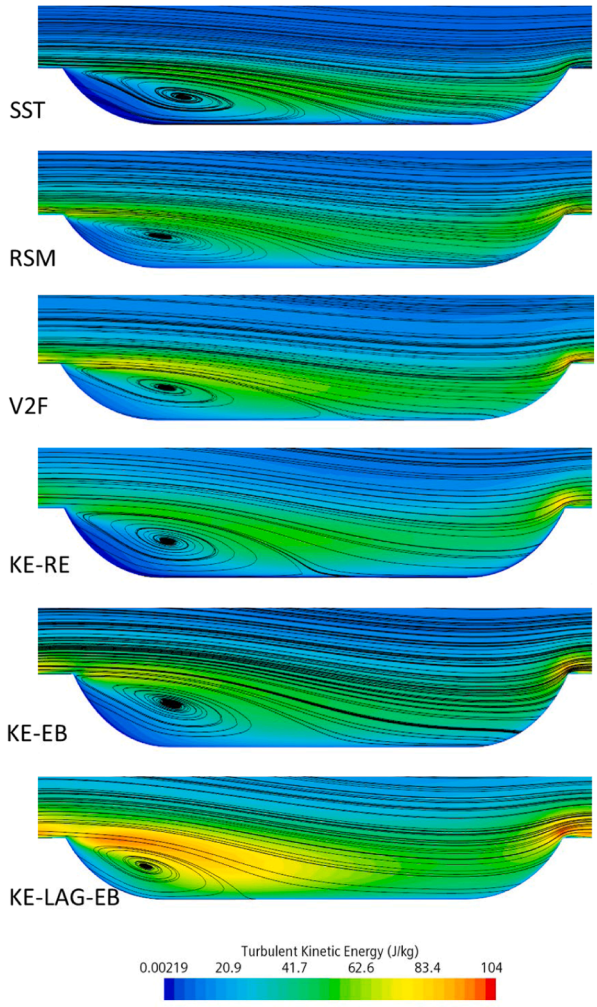

Fig. 17. Flow separation region in the vertical plane section at z=-2mm at the channel length between X= 135 and 150 mm. (Turbulent kinetic energy distribution in the recirculation region visualized by stream lines).

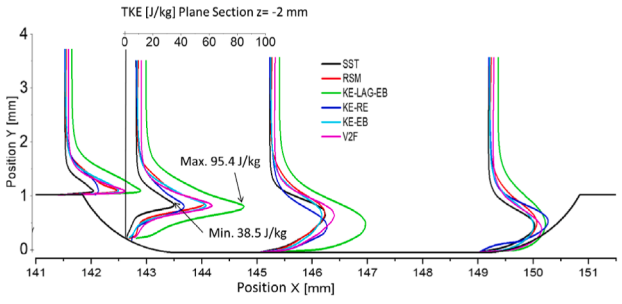

Fig. 18. Turbulent kinetic energy profiles at 4 x-locations: 141.5mm, 142.5 mm, 145 mm, 149 mm.

total intensity of secondary flows relative to the average main flow varies from 15 to 25 %.

All turbulence models both qualitatively and quantitatively show almost the same large-scale vortex structure, which occurs in the entire channel cross-section. Crucial to predicting heat transfer, however, is the correct estimation of the flow behaviour near the wall between the ribs, where the small but intense vortex structures develop. Therefore, the correct prediction of the flow field and turbulence properties in the flow separation region can indicate the suitability of the turbulence models for this type of simulations.

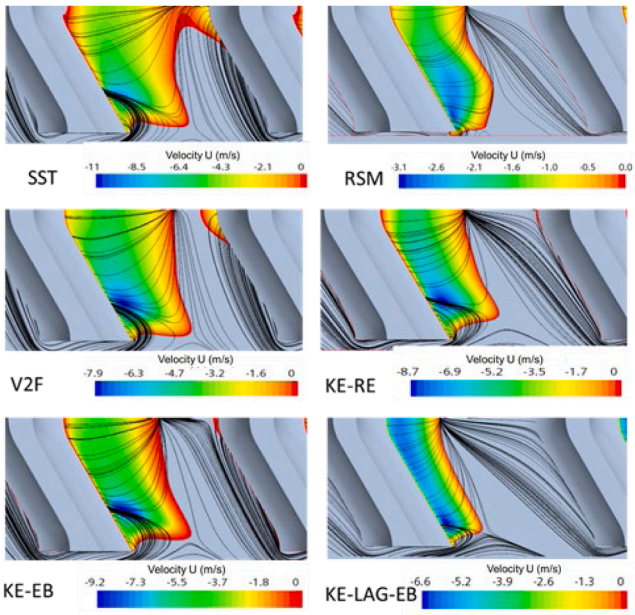

Fig. 19. . Streamlines plane section y=0.05mm, Color scale: velocity *U* (flow direction from left to right). (For interpretation of the references to color in this figure legend, the reader is referred to the web version of this article.).

The difference between the turbulence models becomes clear when comparing the flow separation area in the vertical plane section at z=-2mm at the channel length approximately between x= 135 and 150 mm (middle of the heating length). Fig. 17 shows the turbulent kinetic energy distribution in the recirculation region (visualized by streamlines).

The SST model computes a large recirculation region with a low level of turbulent kinetic energy, which is reflected in the underestimated heat transfer between main and recirculating flow through turbulent mixing. The flow behaviour calculated with KE-RE has slightly larger values of turbulent kinetic energy and noticeably smaller recirculation scope, but most improvements are offered by the RSM, V2F and KE-EB models. Fig. 18 shows the difference in the predicted turbulent kinetic energy profiles in the middle of the channel between the ribs even more clearly.

Fig. 19 shows the visualization of the flow separation area with the streamlines and the color contour of the main velocity in the horizontal plane near the wall (y=0.05 mm). Here it is clearly visible that the flow separation area (*U*-velocity is negative) in the SST simulation extends over the entire area between the ribs, which definitely has a negative effect on the heat transfer. On the contrary, the KE-LAG-EM model calculates the shortest separation range combined with the highest TKE and thus overestimates the heat transfer.

The SST and KE-RE models predict too low Nu number confirming again the inadequacy of these models. It is interesting that both models underestimate the contribution to the heat transfer near the side wall, where the small-scale vortex flows interacts with the large-scale secondary flows.

Fig. 20 compare the ratio between the Nusselt number of the V-ribbed duct and of a smooth channel (Nu/Nu_{h0}) obtained from the HETREX experiments ($Nu_{h0} = 0.023Re^{0.8}Pr^{0.4}$).

6. Conclusions

The applicability of six RANS models implemented in StarCCM+ was examined for the prediction of convective heat transfer and pressure drop in a gas cooling channel with transversally oriented 60° V-shaped ribs on the heated wall.

In the first part of the study, the models were examined for their ability to reproduce the isothermal air flow field in a rectangular

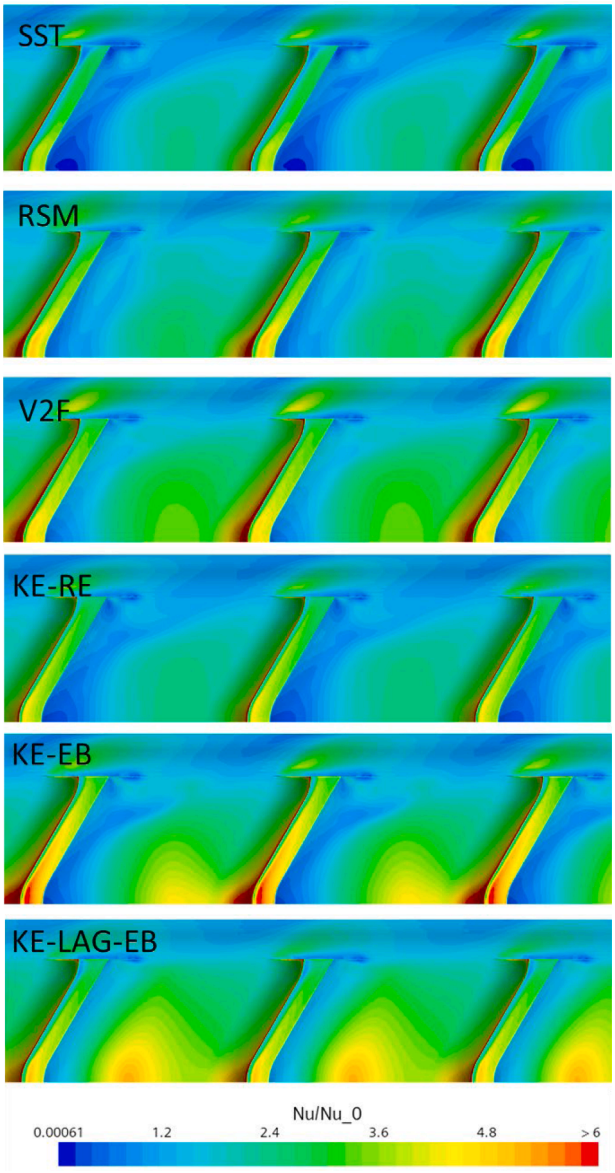

Fig. 20. Nusselt number ratio Nu/Nu_{h0} along the bottom wall, at the channel length between x= 135 and 150 mm.

channel with a transversally ribbed bottom wall [28].

The comparison between flow field measurements and simulations highlights the better performance of RSM, V2F and KE-EB turbulence models compared to KE-RE and KE-LAG-EB models, while the SST model resulted to be practically inadequate.

In the second part, along with comparison of temperature and pressure measurements of HETREX-PT, the development of the flow structures was analysed.

All models reflect roughly the same secondary flow structure.

A comparison between the models shows that the turbulent kinetic energy in the shear flow above recirculation region is lowest for the SST model and highest for the KE-LAG-EB. This difference becomes clear when comparing the flow separation area. The SST model predicts a large recirculation length with a low level of turbulent kinetic energy, reflected in the predicted transfer between main and recirculating flow through turbulent mixing. The KE-RE predicts insignificantly larger turbulence level. Apart from relatively good agreement with the pressure loss measurements in the HETREX-PT experiments, the turbulence and heat transfer data provided by both models cannot be found credible. The comparison results with the straight ribbed channel experiments (Section 3) showed the inability of these models to correctly represent flow behavior in the flow separation area. This is the reason why these models show large disagreement with the measured wall temperatures. Conclusion: both turbulence models are not appropriate for simulation of flow recirculation structures. The KE-LAG-EM model calculates the shortest separation area and thus overestimates the heat transfer. As mentioned in the first part the use of the $C_{\varepsilon 2}$ coefficient as a function of turbulent transport near wall can reduce the turbulence intensity in the shear layer and improve the results of KE-LAG-EB turbulence model.

As shown in comparison with measurements [28] only the RSM, V2F and KE-EB models which can satisfactorily reproduce the flow structure upstream and downstream of the transversal ribs show better agreements with experimental data. The fact that V2F, KE-EB and RSM models show similar simulation results can be explained by relatively equal treatment of the near-wall turbulence using the elliptic blending approach.

The V2F model (together with KE-EB) provides the best overall prediction concerning flow field, pressure drop and global wall temperature profile and is found to be most suitable for the simulation of heat transfer in the presented rib-structured channel flow in application cases that preclude the application of higher fidelity methods like LES.

CRediT authorship contribution statement

S. Gordeev: Investigation. **F. Arbeiter:** Investigation. **S. Ruck:** Investigation.

Declaration of competing interest

The authors declare that they have no known competing financial interests or personal relationships that could have appeared to influence the work reported in this paper.

Acknowledgments

This work has been carried out within the framework of the EUROfusion Consortium, funded by the European Union via the Euratom Research and Training Programme (Grant Agreement No 101052200 - EUROfusion). Views and opinions expressed are however those of the author(s) only and do not necessarily reflect those of the European Union or the European Commission. Neither the European Union nor the European Commission can be held responsible for them.

Data availability

No data was used for the research described in the article.

References

[1] L.V. Boccaccini, et al., Objectives and status of EUROfusion DEMO blanket studies, Fus. Eng. Des. 109–111 (November (Part B)) (2016) 1199–1206.
[2] T.R. Barrett, et al., Progress in the engineering design and assessment of the European DEMO first wall and divertor plasma facing components, Fus. Eng. Des. 109–111 (November (Part A)) (2016) 917–924.
[3] F. Arbeiter, et al., Options for a high heat flux enabled helium cooled first wall for DEMO, Fus. Eng. Des. 119 (2017) 22–28.
[4] S. Ruck, et al., Thermal-hydraulic study on rib and dimple structures for cooling the First Wall of DEMO, Fus. Eng. Des. 146 (Part B) (2019) 2144–2148.
[5] S.C. Lau, R.T. Kukreja, D.R. McMillin, Effects of V-shaped rib arrays on turbulent heat transfer and friction of fully developed flow in a square channel, Int. J. Heat Mass Transf. 34 (7) (1991) 1605–1616.
[6] M.E. Taslim, T. Li, D.M. Kercher, Experimental heat transfer and friction in channels roughened with angled, V-shaped, and discrete ribs on two opposite walls, ASME J. Turbomach. 118 (1996) 20–28.
[7] M.E. Taslim, T. Li, D.M. Kercher, Experimental heat transfer and friction in channels roughened with angled, V-shaped, and discrete ribs on two opposite walls, ASME J. Turbomach. 118 (1996) 20–28.
[8] N. Kaewchoothong, K. Maliwan, K. Takeishi, C. Nuntadusit, Effect of inclined ribs on heat transfer coefficient in stationary square channel, Theor. Appl. Mech. Lett. 7 (2017) 344–350.

[9] F. Arbeiter, S. Ruck, T. Böttcher, G. Schlindwein, K. Zinn, Final Report on Deliverable Enhanced heat transfer characteristics of helium cooled channel flows: Test section design EUROfusion IDM EFDA_D_2MDYJN, Version 1.0, 10-Dec-14.
[10] S. Ruck, G. Schlindwein, K. Zinn, F. Arbeiter, Final Report on Deliverable Report on Study of Enhanced Cooling Channel Geometries (Helium), EUROfusion IDM EFDA_D_2NDF2G Version: 1.2 29-Jan-2018.
[11] © 2021 Siemens. Simcenter STAR-CCM+ 2021.2 Build 16.04.007.
[12] F.R. Menter, Two-equation eddy-viscosity turbulence modeling for engineering applications, AIAA J. 32 (8) (1994) 1598–1605.
[13] T.-H. Shih, et al., A New k-ε Eddy Viscosity Model for High Reynolds Number Turbulent Flows – Model Development and Validation, 1994. NASA TM 106721.
[14] P.A. Durbin, On the k-e stagnation point anomaly, Int. J. Heat Fluid Flow 17 (1996) 89–90.
[15] P. A. Durbin, Separated flow computations with the k-epsilon-v-squared model, Volume 33, Number 4, April 1995.
[16] G. Kalitzin, Application of the v2-f Model to Aerospace Configurations, Center for Turbulence Research Annual Research Briefs, 1999.
[17] S. Parneix, P.A. Durbin, M. Behnia, Computation of three-dimensional turbulent boundary layers using the v 2 –f model, Flow Turbul. Combust. 60 (1998) 19–46.
[18] G. Iaccarino, Predictions of a turbulent separated flow using commercial CFD codes, J. Fluids Eng. 123 (4) (2001) 819–828.
[19] D. Cokljat, S.E. Kim, G. Iaccarino, P. Durbin, A comparative assessment of the V2F model for recirculating flows, in: 41st Aerospace Sciences Meeting and Exhibit, 2003.
[20] P.A. Durbin, Application of a near-wall turbulence model to boundary layers and heat transfer, Int. J. Heat Fluid Flow 14 (4) (1993) 316–323.
[21] F. Billard, D. Laurence, A robust k−ε-v2/k elliptic blending turbulence model applied tonear-wall, separated and buoyant flows, Int. J. Heat Fluid Flow 33 (1) (2012) 45–58.
[22] S. Lardeau, F. Billard, Development of an elliptic-blending lag model for industrial applications, in: 54th AIAA Aerospace Sciences Meeting, 2016, p. 1600.
[23] Remi Manceau, Kemal Hanjalić, Elliptic blending model: a new near-wall Reynolds-stress turbulence closure, Phys. Fluids 14 (2) (2002) 744–754.
[24] K. Hanjalić, B.E. Launder, A Reynolds stress model of turbulence and its application to thin shear flows, J. Fluid Mech. 52 (4) (1972) 609–638.
[25] B.E. Launder, G.J. Reece, W. Rodi, Progress in the development of a Reynolds-stress turbulence closure, J. Fluid Mech. 68 (3) (1975) 537–566.
[26] Y. Lai, Computational method of second-moment closure in complex geometries, AIAA J. 33 (8) (1995) 1426–1432.
[27] D.R. Launchbury, L. Mangani, E. Casartelli, F.D. Citto, A robust implementation of a reynolds stress model for turbomachinery applications in a coupled solver environment, J. Turbomach. 143 (9) (2021).
[28] S. Ruck, F. Arbeiter, LDA measurements in a one-sided ribbed square channel at Reynolds numbers of 50,000 and 100,000, Exp. Fluids 62 (2021) 232, https://doi.org/10.1007/s00348-021-03313-5.
[29] S. Ruck, S. Köhler, G. Schlindwein, F. Arbeiter, Heat transfer and pressure drop measurements in channels roughened by variously shaped ribs on one wall, Exp. Heat Transf. 31 (4) (2017) 334–354, https://doi.org/10.1080/08916152.2017.1410506.
[30] J. Jeong, F. Hussain, On the identification of a vortex, J. Fluid Mech. 285 (1995) 69–94.